JACS
JOURNAL OF THE AMERICAN CHEMICAL SOCIETY
Communication
pubs.acs.org/JACS

Metal–Macrocycle Framework (MMF): Supramolecular Nano-Channel Surfaces with Shape Sorting Capability

Shohei Tashiro, Ryou Kubota, and Mitsuhiko Shionoya*

Department of Chemistry, Graduate School of Science, The University of Tokyo, 7-3-1 Hongo, Bunkyo-ku, Tokyo 113-0033, Japan

Supporting Information

ABSTRACT: Hollow nanostructures for the functional assembly of chemical groups with inner surface geometry and regulable stoichiometry enable steric design of interior reaction centers. Herein we report a metal–macrocycle framework (MMF) that forms single-crystalline nanochannels with five distinct enantiomeric pairs of guest binding pockets. During crystal-soaking experiments, the MMF crystals can encapsulate aromatic molecules with high site selectivity. First, constitutional isomers of dibromobenzene are captured and sorted into different binding pockets. Second, each of the optical isomers of (1*R*/1*S*)-1-(3-chlorophenyl)ethanol is included diastereoselectively into one of an enantiomeric pair of binding pockets. An advantage of this strategy is that the interior walls can be "repainted" via replacement of the trapped molecules with alternatives. Such guest uptake behaviors would allow highly regioselective or stereoselective reactions within the nanochannel.

Hollow structures within self-assembled molecular aggregates such as capsules,[1−3] vesicles/micelles,[4] tubes,[5] and porous materials[6−14] provide platforms for molecular arrangement, separation, storage, transport, and catalysis. A key factor in their further development is to be able to upgrade and integrate the functions of the interior surfaces within the aggregates based on the characteristics of the building blocks. A promising strategy for this approach is to arrange different receptor molecules as their internal walls that can be postfunctionalized by site-selective guest encapsulation into the host cavities.

Porous crystalline materials such as metal–organic frameworks (MOFs), zeolites, and organic crystals exhibit spatially dependent capabilities for gas adsorption, separation, proton conductance, molecular arrangement, catalysis, and space-specific reactions.[6−14] However, the design of the interior surfaces of these hollow structures is at an early stage of investigation, and so far only a few examples of covalently premodified[15−17] or postmodified[18−20] MOFs with a single functionality, and of noncovalently postfunctionalized MOFs with recognition sites on their skeletons,[21−23] have been reported. Recently, Yaghi reported outstanding MOFs with multifunctionalized pores.[24] In our efforts for creating diversely functionalized spaces, we envisioned that self-organization of receptor molecules would provide an isolated space for multiple guest binding sites based on the host properties. A receptor molecule used for this purpose was a trinuclear Pd^{II} complex with a single macrocycle **1**. This complex forms a single-crystalline nanochannel in CH_3CN with an internal diameter of ca. 1.5 nm through intermolecular H-bonding and Pd–Pd interactions. The resulting channel, in spite of its one-component system, provides five enantiomerically paired guest binding pockets in a basic structural unit, which vary in size, shape, and chirality due to the generation of (i) two conformational isomers (*Syn* and *Anti*), (ii) intramolecular CH-π bonding leading to helicity with paired enantiomers (*P* and *M*), (iii) a pair of head and tail cavities of each isomer of the Pd^{II} complex, and (iv) interspatial pockets outside the macrocycles. As a result, this metal–macrocycle framework (MMF) leads to site-selective guest inclusion within the interior channel surfaces.

A promising approach to nanochannel construction with multiple recognition sites is self-assembly of receptor molecules while retaining or improving their host properties. So far, several macrocycles such as calixarene,[25,26] cyclodextrin,[27] cucurbituril,[28] metal-macrocycle,[29] and cages[30,31] have been utilized as building blocks for channel skeletons, and the resulting channels exhibit unique guest uptake capabilities. However, it would seem to be difficult to construct recognition sites of great variety within the channel from a single macrocycle.

The complexation of macrocycle **1** with 3 equiv of $PdCl_2(CH_3CN)_2$ in CH_3CN simultaneously generates yellow single-crystals composed of four structural isomers of a neutral, trinuclear Pd^{II} complex, $Pd_3\mathbf{1}Cl_6$, in 41% yield. The resulting crystals are thermally stable up to 220 °C as confirmed by thermogravimetric analysis (Figure S4, Supporting Information). A single-crystal X-ray analysis revealed a molecular structure composed of four structural isomers of $Pd_3\mathbf{1}Cl_6$, (*P*)-*Syn*, (*M*)-*Syn*, (*P*)-*Anti*, and (*M*)-*Anti* isomers, in the same molar ratio (Figure 1a–f). In the *Syn* or *Anti* isomer, all three or two of the three Pd^{II} centers are on one side of their cavity, respectively. Moreover, an enantiomeric pair of helical structures (*P* and *M*) is generated due to the intramolecular circularly oriented three-point CH-π interactions between methylene and phenylene groups of the macrocycle (Figure 1e,f). As a result, in light of both sides of the macrocyclic plane (head-Pocket and tail-Pocket), the above-mentioned four isomers potentially provide eight different binding pockets (Figure 1a–d).

Notably, the four isomers of $Pd_3\mathbf{1}Cl_6$ are regularly arranged to form a large honeycombed channel structure along the *c*-axis

Received: October 6, 2011
Published: December 13, 2011

   dx.doi.org/10.1021/ja209422m | *J. Am. Chem.Soc.* 2012, 134, 2461–2464

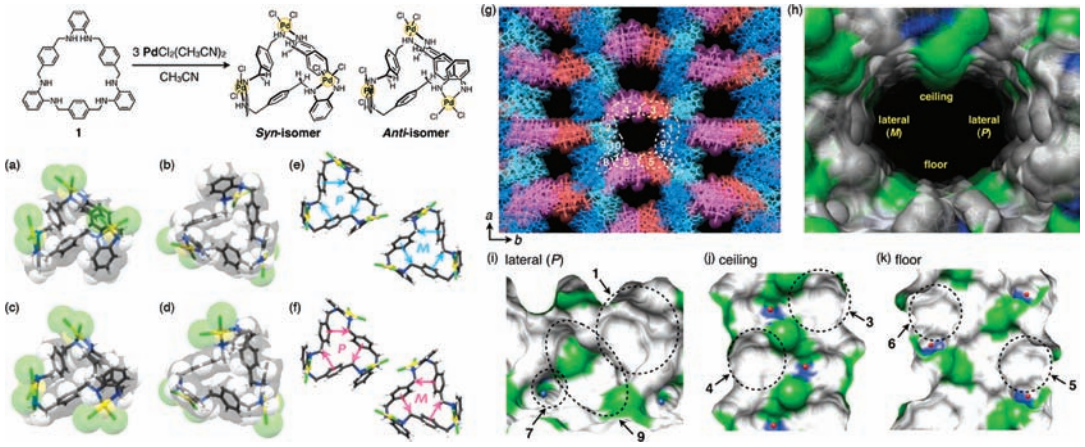

Figure 1. Self-organization of four structural isomers of Pd_3**1**Cl_6 into a single-crystalline nanochannel. Overhead views of (a) *Syn*-head-Pocket, (b) *Syn*-tail-Pocket, (c) *Anti*-head-Pocket, and (d) *Anti*-tail-Pocket of the (*P*)-isomer of Pd_3**1**Cl_6. Top views of (e) (*P*/*M*)-*Syn*-isomers and (f) (*P*/*M*)-*Anti*-isomers. The resulting helical senses (*P*/*M*) are defined based on the direction of CH−π interactions denoted as arrows. Pd, yellow; Cl, green; C, gray; H, white. (g) Crystal packing structure. (*P*)-*Syn*, (*M*)-*Syn*, (*P*)-*Anti*, and (*M*)-*Anti* isomers are represented by *blue*, *cyan*, *red*, and *pink*, respectively. Solvent-excluded molecular surfaces of the (h) channel, (i) lateral (*P*) with one CH_3CN bound to the Tubular-Pocket, (j) ceiling, and (k) floor with bound H_2O molecules shown as red spheres. The CH_3CN molecules tightly bound to the Tubular-Pocket were not replaced by any guest molecules tested. Exposed Cl and N−H groups are represented by *green* and *blue*, respectively. The numbers with circles denote binding pockets of a unit pore; 1, (*P*)-*Syn*-tail-Pocket; 2, (*M*)-*Syn*-tail-Pocket; 3, (*P*)-*Anti*-head-Pocket; 4, (*M*)-*Anti*-head-Pocket; 5, (*P*)-*Anti*-tail-Pocket; 6, (*M*)-*Anti*-tail-Pocket; 7, (*P*)-Tubular-Pocket; 8, (*M*)-Tubular-Pocket; 9, (*P*)-Ellipsoidal-Pocket; 10, (*M*)-Ellipsoidal-Pocket, where (*P*)- and (*M*)-Tubular(Ellipsoidal)-Pockets are enantiomeric with each other. For ease of definition, the voids located in (*P*)- and (*M*)-rich areas are denoted by (*P*)- and (*M*)-forms, respectively.

with a rectangular pore size of 1.9 × 1.4 nm (Figure 1g). Eight molecules of Pd_3**1**Cl_6 forming two pores are included in a unit cell. The PLATON analysis showed that the solvent-accessible volume of the crystal is ca. 44%, suggesting that the volume of one pore in the unit cell is 6292 Å^3. A honeycombed porous structure projected along the *c*-axis can be described by the two patterns of assemblies, that is, the formation of 2D-infinite sheets from (*P*/*M*)-*Syn*-isomers along the *ac*-plane (Figure 1g, blue and cyan parts) and the formation of 1D-infinite slats ca. 1.8 nm wide from (*P*/*M*)-*Anti*-isomers along the *c*-axis (Figure 1g, red and pink parts), through multiple H-bonds and Pd−Pd interactions.[32] The 2D-infinite sheets are arranged parallel to each other at intervals of ca. 2 nm and perpendicularly joined with the 1D-infinite slats to construct a honeycombed channel packing structure.

As a result of the cocrystallization of four isomers of Pd_3**1**Cl_6, the single-crystalline channel can provide chemically and optically different multiple binding pockets on the interior surfaces (Figure 1g,h). Specifically, an enantiomeric pair of two head pockets ((*P*)-*Anti*-head-Pocket and (*M*)-*Anti*-head-Pocket) is arranged on the ceiling surface of the channel (Figure 1j), whereas on the floor surface an enantiomeric pair of two tail pockets ((*P*)-*Anti*-tail-Pocket and (*M*)-*Anti*-tail-Pocket) is arranged (Figure 1k). In contrast, the two lateral walls are constructed by (*P*)-*Syn* and (*M*)-*Syn* isomers, and therefore the channel is fenced in by an enantiomeric pair of (*P*/*M*)-*Syn*-tail-Pockets on each side (Figure 1h,i). Unlike these pockets, the remaining (*P*/*M*)-*Syn*-head-Pockets do not face toward the interior space but are buried in the channel skeleton. Besides these macrocyclic pockets, two "Tubular-Pockets" are formed at the aperture of two *Syn* and one *Anti* isomers, where one CH_3CN molecule is deeply buried (Figure 1i). Furthermore, the other two "Ellipsoidal-Pockets" are found surrounded by *Syn* and *Anti* isomers (Figure 1i). In addition to these hydrophobic pockets, there are several hydrophilic channel surface areas. Specifically, Cl^- ligands bound to Pd^{II} ions are linearly arranged on the channel ceiling surface at intervals of 7.2 Å (Figure 1j). Furthermore, on the opposite floor surface Cl^- groups are similarly arranged in two lines in a zigzag manner (Figure 1k). These Cl^- ions form H-bonds with bound H_2O molecules on the channel surfaces.

We examined the guest uptake behavior within the nanochannel. The crystals were soaked in a mixture of CH_3CN and benzene. The X-ray analysis of the resulting single-crystals indicates that benzene molecules are clearly identified in four binding pockets, (*P*/*M*)-*Syn*-tail-Pockets and (*P*/*M*)-*Anti*-head-Pockets (Figure 2a), where CH−π interactions are observed between benzene and macrocycle **1**. Similarly, bicyclic naphthalene and azulene are also included into four binding pockets: (*P*/*M*)-*Syn*-tail-Pockets and (*P*/*M*)-Ellipsoidal-Pockets (Figure 2b,c).

To further assess the site-selectivity and orientation of bound guest, we compared the binding of three constitutional isomers of dibromobenzene. The crystals were soaked in a CH_3CN solution containing *o*-, *m*-, or *p*-dibromobenzene (2.8, 2.8 M, or saturated solution, respectively) under similar conditions to benzene inclusion. The X-ray analyses of the resulting single-crystals revealed that each dibromobenzene isomer is captured site-selectively by a specific binding pocket with a high shape-dependence. Indeed, *o*-dibromobenzene molecules are included in four binding pockets: (*P*/*M*)-*Syn*-tail-Pockets and (*P*/*M*)-Ellipsoidal-Pockets (Figure 2d), while *m*-dibromobenzene molecules are captured by the four macrocyclic pockets: (*P*/*M*)-*Syn*-tail-Pockets and (*P*/*M*)-*Anti*-head-Pockets (Figure 2e). In contrast, *p*-dibromobenzene molecules are trapped neither in (*P*/*M*)-*Syn*-tail-Pockets nor in (*P*/*M*)-*Anti*-head-Pockets, but are found in the (*P*/*M*)-Ellipsoidal-Pockets (Figure 2f). Notably, the bound dibromobenzene molecules are not disordered and anchored in each pocket, as was confirmed by the positions of heavy Br atoms.

Subsequently, we conducted crystal-soaking experiments using a mixture of *m*- and *p*-dibromobenzene in CH_3CN. As

dx.doi.org/10.1021/ja209422m | *J. Am. Chem.Soc.* 2012, 134, 2461−2464

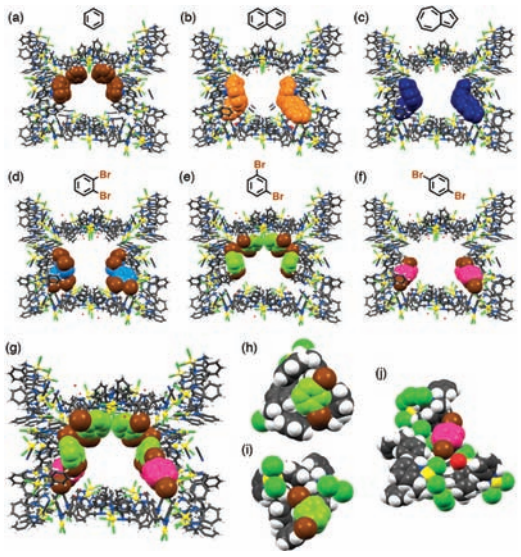

Figure 2. Site-selective uptake of benzene, naphthalene, azulene, or constitutional isomers of dibromobenzene into the multibinding pockets of the channel. Channel structures of Pd_31Cl_6 crystals soaked in (a) a 1:1 mixture of benzene and CH_3CN, (b) a saturated CH_3CN solution of naphthalene, or (c) a CH_3CN solution containing azulene (0.3 M). The trapped benzene molecules in (*P*/*M*)-*Anti*-head- and (*P*/*M*)-*Syn*-tail-Pockets (82 and 66%, respectively), naphthalene molecules in (*P*/*M*)-*Syn*-tail- and (*P*/*M*)-Ellipsoidal-Pockets (65 and 74%, respectively), or azulene molecules in (*P*/*M*)-*Syn*-tail- and (*P*/*M*)-Ellipsoidal-Pockets (100 and 59%, respectively) are represented by *brown*, *orange*, or *dark blue* colored space-filling models, respectively. Channel structures of Pd_31Cl_6 crystals soaked in a CH_3CN solution of (d) *o*-, (e) *m*-, or (f) *p*-dibromobenzene. The captured *o*-isomer molecules in (*P*/*M*)-*Syn*-tail- and (*P*/*M*)-Ellipsoidal-Pockets (51 and 53%, respectively), *m*-isomer molecules in (*P*/*M*)-*Syn*-tail- and (*P*/*M*)-*Anti*-head-Pockets (52 and 89%, respectively), or *p*-isomer molecules in (*P*/*M*)-Ellipsoidal-Pockets (68%). These are represented by space-filling models with *blue*, *green*, or *pink* colored carbon atoms, respectively. (g) Channel structure of Pd_31Cl_6 crystals soaked in a CH_3CN solution containing *m*- and *p*-dibromobenzene (0.96 M each). Inclusion structures of *m*-dibromobenzene in (h) (*P*)-*Syn*-tail-Pocket (45%) or (i) (*M*)-*Anti*-head-Pocket (75%), and (j) *p*-dibromobenzene in (*M*)-Ellipsoidal-Pocket (69%). The molecular occupancies are in the parentheses.

a result, the two isomers were selectively sorted into different binding pockets (Figure 2g–j). Indeed, *m*-isomer molecules are included in the (*P*/*M*)-*Syn*-tail-Pockets (Figure 2h) and (*P*/*M*)-*Anti*-head-Pockets (Figure 2i), and *p*-isomer molecules are captured in the (*P*/*M*)-Ellipsoidal-Pockets (Figure 2j). No other *m*- and *p*-isomers are found anywhere in the remaining part of the channel surfaces. Thus, this guest binding selectivity observed with the mixture is completely consistent with the implications of the observations made previously with each individual isomer.

Furthermore, all three constitutional isomers of dibromobenzene together were tested using a similar protocol, leading to a result quite similar to that with the coencapsulation of *m*- and *p*-isomers. Notably, the *o*-isomer molecules were only found in (*P*/*M*)-*Syn*-tail-Pockets with a very low occupancy. This result indicates that *m*- and *p*-dibromobenzene preferentially bind to the (*P*/*M*)-*Syn*-tail- and (*P*/*M*)-Ellipsoidal-Pockets.

The composition of disordered molecules included in the free channel space was quantified by elemental analysis of the soaked crystals and by ^{1}H NMR study of the digestion product in DMSO-d_6/DCl-D_2O. For example, crystals soaked in a CH_3CN solution of *m*-dibromobenzene (2.8 M) contain approximately nine molecules of *m*-dibromobenzene in the free space per unit pore, suggesting that the disordered *m*-dibromobenzene molecules occupy ca. 50% of the free space volume. The remaining channel spaces appear to contain solvent molecules such as CH_3CN and H_2O.

In addition to the site-selective guest recognition, diastereoselective guest binding also takes place when using an optically pure guest molecule. First, a *meta*-substituted chlorobenzene derivative, (1*S*)-1-(3-chlorophenyl)ethanol, was used for the soaking experiment (Figure 3a). The X-ray

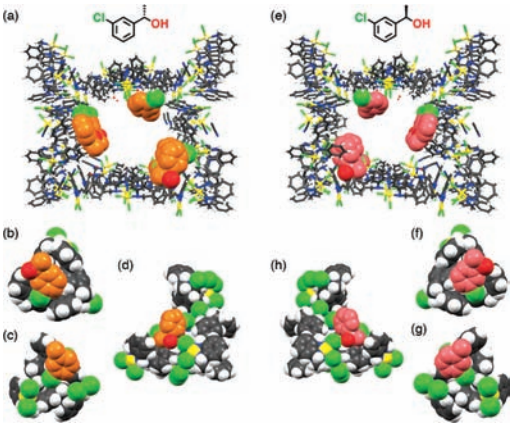

Figure 3. Highly diastereoselective uptake of (1*S*)- or (1*R*)-1-(3-chlorophenyl)ethanol. (a) Crystal packing structure of Pd_31Cl_6 crystals soaked in a CH_3CN solution containing (1*S*)-1-(3-chlorophenyl)-ethanol (5.0 M). The captured molecules are represented by space-filling models with orange colored carbon atoms. Inclusion structures of (1*S*)-1-(3-chlorophenyl)ethanol in (b) (*M*)-*Syn*-tail-Pocket (91% occupancy), (c) (*P*)-*Anti*-head-Pocket (94% occupancy), and (d) (*P*)-Ellipsoidal-Pocket (75% occupancy). (e) Crystal packing structure of Pd_31Cl_6 crystals soaked in a CH_3CN solution containing (1*R*)-1-(3-chlorophenyl)ethanol (5.0 M). The captured molecules are represented by space-filling models with pink colored carbon atoms. Inclusion structures of (1*R*)-1-(3-chlorophenyl)ethanol in (f) (*P*)-*Syn*-tail-Pocket (76% occupancy), (g) (*M*)-*Anti*-head-Pocket (100% occupancy), and (h) (*M*)-Ellipsoidal-Pocket (75% occupancy).

analysis of the resulting crystal revealed that the chiral guest molecules are highly diastereoselectively captured only in one of the enantiomerically paired binding pockets, specifically the (*M*)-*Syn*-tail-Pocket, (*P*)-*Anti*-head-Pocket, and (*P*)-Ellipsoidal-Pocket (Figure 3b–d). Notably, no significant electron density of the guest was observed in the mirror-image, enantiomeric pockets, suggesting that the resulting diastereoselectivity is substantial. As is obvious, (1*R*)-isomer molecules are trapped only in the (*P*)-*Syn*-tail-Pocket, (*M*)-*Anti*-head-Pocket, and (*M*)-Ellipsoidal-Pocket (Figure 3e–h). As for (*rac*)-1-(3-chlorophenyl)ethanol, no diastereoselectivity is observed and the guest molecules are captured only in the (*P*/*M*)-*Syn*-tail-Pockets due to the steric hindrance (Figure S30, Supporting Information).

Finally, we visually observed reversible guest uptake and release with colored guests, methyl orange (in H_2O) and azulene (in CH_3CN). When the crystals are soaked in an aqueous solution of methyl orange, the yellow color of crystals changes anisotropically to red along the channel direction from both ends of the crystal (Figure 4a–d). Azulene is also taken up

dx.doi.org/10.1021/ja209422m | *J. Am. Chem.Soc.* 2012, 134, 2461–2464

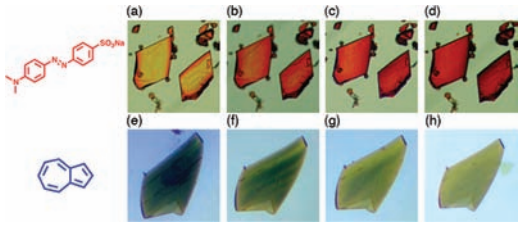

Figure 4. Pictures of crystals including methyl orange and azulene. Anisotropic uptake of methyl orange into the channel: the crystals were soaked in a saturated, neutral aqueous solution of methyl orange for (a) 5 min, (b) 1, (c) 8, and (d) 31 h. Azulene (0.68 M in CH_3CN) was also uptaken into the channel of the crystals and quickly released when soaked in CH_3CN for (e) 0, (f) 1, (g) 2, and (h) 3 min.

into the channel and the color changes to blue (Figure 4e). Importantly, the captured molecules are easily removed to regenerate the original crystals by soaking in CH_3CN (Figure 4e–h). Thus, the guest molecules can be easily recovered and the interior surfaces of the MMF can be "repainted".[33]

In conclusion, an MMF with supramolecular nanochannels formed from a single macrocyclic Pd^{II} complex exhibits highly shape-specific, site-selective guest binding to different recognition sites on the channel surfaces. The captured molecules can be easily recovered by soaking in a solvent to regenerate the original crystals. This shape sorting capability of our MMF would enable not only direct molecular recognition or separation but also functional integration by site-selective fixation of anchor molecules, through a tethered phenyl derivative, to a particular binding site. Therefore, this system is expected to establish a novel method for creating precise molecular arrays leading to multifunctional catalytic centers and to controlled organic and inorganic polymerization.

■ ASSOCIATED CONTENT

Supporting Information

All experimental procedures and data, and X-ray crystallographic data (CIF). This material is available free of charge via the Internet at http://pubs.acs.org.

■ AUTHOR INFORMATION

Corresponding Author

shionoya@chem.s.u-tokyo.ac.jp

■ ACKNOWLEDGMENTS

This research was supported in part by Global COE Program, Chemistry Innovation through Cooperation of Science and Engineering, and KAKENHI, the Japan Society for the Promotion of Science and MEXT, Japan. We thank Dr. J.-L. Duprey for his helpful discussion. We are grateful to Takasago International Corporation for kind provision of (1*R*)-1-(3-chlorophenyl)ethanol.

■ REFERENCES

(1) Rebek, J. Jr. *Angew. Chem., Int. Ed.* **2005**, *44*, 2068–2078.
(2) Caulder, D. L.; Raymond, K. N. *Acc. Chem. Res.* **1999**, *32*, 975–982.
(3) Yoshizawa, M.; Klosterman, J. K.; Fujita, M. *Angew. Chem., Int. Ed.* **2009**, *48*, 3418–3438.
(4) Discher, D. E.; Eisenberg, A. *Science* **2002**, *297*, 967–973.
(5) Shimizu, T.; Masuda, M.; Minamikawa, H. *Chem. Rev.* **2005**, *105*, 1401–1443.
(6) Yaghi, O. M.; O'Keeffe, M.; Ockwig, N. W.; Chae, H. K.; Eddaoudi, M.; Kim, J. *Nature* **2003**, *423*, 705–714.
(7) Kitagawa, S.; Kitaura, R.; Noro, S. *Angew. Chem., Int. Ed.* **2004**, *43*, 2334–2375.
(8) Férey, G. *Chem. Soc. Rev.* **2008**, *37*, 191–214.
(9) Dincă, M.; Long, J. R. *Angew. Chem., Int. Ed.* **2008**, *47*, 6766–6779.
(10) Bradshaw, D.; Claridge, J. B.; Cussen, E. J.; Prior, T. J.; Rosseinsky, M. J. *Acc. Chem. Res.* **2005**, *38*, 273–282.
(11) Rowsell, J. L. C.; Spencer, E. C.; Eckert, J.; Howard, J. A. K.; Yaghi, O. M. *Science* **2005**, *309*, 1350–1354.
(12) Férey, G.; Mellot-Draznieks, C.; Serre, C.; Millange, F.; Dutour, J.; Surblé, S.; Margiolaki, I. *Science* **2005**, *309*, 2040–2042.
(13) Côté, A. P.; Benin, A. I.; Ockwig, N. W.; O'Keeffe, M.; Matzger, A. J.; Yaghi, O. M. *Science* **2005**, *310*, 1166–1170.
(14) Van Bekkum, H., Flanigen, E. M., Jacobs, P. A., Jansen, J. C., Eds. *Introduction to Zeolite Science and Practice*; Elsevier: Amsterdam, 2001.
(15) Matsuda, R.; Kitaura, R.; Kitagawa, S.; Kubota, Y.; Belosludov, R. V.; Kobayashi, T. C.; Sakamoto, H.; Chiba, T.; Takata, M.; Kawazoe, Y.; Mita, Y. *Nature* **2005**, *436*, 238–241.
(16) Farha, O. K.; Shultz, A. M.; Sarjeant, A. A.; Nguyen, S. T.; Hupp, J. T. *J. Am. Chem. Soc.* **2011**, *133*, 5652–5655.
(17) Shimomura, S.; Horike, S.; Matsuda, R.; Kitagawa, S. *J. Am. Chem. Soc.* **2007**, *129*, 10990–10991.
(18) Seo, J. S.; Whang, D.; Lee, H.; Jun, S. I.; Oh, J.; Jeon, Y. J.; Kim, K. *Nature* **2000**, *404*, 982–986.
(19) Wang, Z.; Cohen, S. M. *Chem. Soc. Rev.* **2009**, *38*, 1315–1329.
(20) Kawamichi, T.; Haneda, T.; Kawano, M.; Fujita, M. *Nature* **2009**, *461*, 633–635.
(21) Li, Q.; Zhang, W.; Miljanić, O. Š.; Sue, C.-H.; Zhao, Y.-L.; Liu, L.; Knobler, C. B.; Stoddart, J. F.; Yaghi, O. M. *Science* **2009**, *325*, 855–859.
(22) Chui, S. S.-Y.; Lo, S. M.-F.; Charmant, J. P. H; Orpen, A. G.; Williams, I. D. *Science* **1999**, *283*, 1148–1150.
(23) Ma, L.; Wu, C.-D.; Wanderley, M. M.; Lin, W. *Angew. Chem., Int. Ed.* **2010**, *49*, 8244–8248.
(24) Deng, H.; Doonan, C. J.; Furukawa, H.; Ferreira, R. B.; Towne, J.; Knobler, C. B.; Wang, B.; Yaghi, O. M. *Science* **2010**, *327*, 846–850.
(25) Orr, G. W.; Barbour, L. J.; Atwood, J. L. *Science* **1999**, *285*, 1049–1052.
(26) Hong, B. H.; Bae, S. C.; Lee, C.-W.; Jeong, S.; Kim, K. S. *Science* **2001**, *294*, 348–351.
(27) Smaldone, R. A.; Forgan, R. S.; Furukawa, H.; Gassensmith, J. J.; Slawin, A. M. Z.; Yaghi, O. M.; Stoddart, J. F. *Angew. Chem., Int. Ed.* **2010**, *49*, 8630–8634.
(28) Kim, H.; Kim, Y.; Yoon, M.; Lim, S.; Park, S. M.; Seo, G.; Kim, K. *J. Am. Chem. Soc.* **2010**, *132*, 12200–12202.
(29) Williams, M. E.; Benkstein, K. D.; Abel, C.; Dinolfo, P. H.; Hupp, J. T. *Proc. Natl. Acad. Sci. U.S.A.* **2002**, *99*, 5171–5177.
(30) Inokuma, Y.; Arai, T.; Fujita, M. *Nat. Chem.* **2010**, *2*, 780–783.
(31) Jones, J. T. A.; Hasell, T.; Wu, X.; Bacsa, J.; Jelfs, K. E.; Schmidtmann, M.; Chong, S. Y.; Adams, D. J.; Trewin, A.; Schiffman, F.; Cora, F.; Slater, B.; Steiner, A.; Day, G. M.; Cooper, A. I. *Nature* **2011**, *474*, 367–371.
(32) Specifically, 36 classical H-bonds between complexes and complex/water, 20 nonclassical H-bonds (16 C–H---Cl and 4 N–H---π), and two sets of Pd–Pd interactions (3.42 Å) with 2 H-bonds (N–H---Cl–Pd) for each construct a unit cell.
(33) Preserving the single crystallinity of crystals after guest release was confirmed by the XRD measurement. Specifically, crystals including (1*S*)-1-(3-chlorophenyl)ethanol in the pore were washed with CH_3CN, then soaked in CH_3CN for 1 day. The single-crystal X-ray analysis of the resulting crystal revealed that no (1*S*)-1-(3-chlorophenyl)ethanol molecules were found in the pore.